




Adaptive model for the optical properties of excited goldP. D. Ndione ^{1,*}, S. T. Weber ¹, D. O. Gericke ² and B. Rethfeld ¹¹*Department of Physics and OPTIMAS Research Center, RPTU Kaiserslautern-Landau, Erwin-Schrödinger-Straße 46, 67663 Kaiserslautern, Germany*²*Centre for Fusion, Space, and Astrophysics, Department of Physics, University of Warwick, Coventry CV4 7AL, United Kingdom* (Received 26 July 2023; revised 1 December 2023; accepted 21 February 2024; published 22 March 2024)

We investigate the optical properties of laser-excited gold within the Drude-Lorentz framework. Our approach extends the Drude-Lorentz model, initially fitted to experimental data for ambient conditions, to accommodate higher temperatures. It covers a wide range of excitation strengths and frequencies, Fermi-distributed electrons, as well as nonequilibrium scenarios. It is in good qualitative agreement with density functional theory–based calculations capturing key features of the reflectivity and, thus, provides a very efficient alternative to these numerically expensive calculations. When applied to thin films, we find a nonlinear dependence of reflection and absorption on electron temperature, accentuated at lower photon energies and under polarized light. Our highly efficient model can be particularly valuable when analyzing experiments investigating ultrafast processes as the pathways of energy relaxation in laser-excited samples.

DOI: [10.1103/PhysRevB.109.115148](https://doi.org/10.1103/PhysRevB.109.115148)**I. INTRODUCTION**

The optical response of materials has been subject to extensive studies over the last decades due to its potential application in various fields, including plasmonics [1,2], material processing [3], and optoelectronics [4]. Optical properties are also often used for diagnostics and thus play a crucial role in our understanding of the fundamental properties of matter. For example, the electron kinetics in condensed matter has been investigated by reflectivity and/or transmissivity measurements [5–7]. Similarly, a combination of optical probing [8,9] and modeling [10,11] has been used to provide valuable quantitative benchmarks of important properties such as the electron-phonon coupling strength in warm dense matter.

Laser excitation of matter can strongly modify the energy distribution of the electrons, changing its optical properties, which creates a feedback mechanism to the absorption process. Thus, an accurate description of the transient energy deposition requires an appropriate evaluation of the time-dependent dielectric function. Near equilibrium, it can be provided by *ab initio* methods such as density functional theory (DFT) via the Kubo-Greenwood formula [11–15]. Unfortunately, these methods are not always applicable due to their high computational costs. Moreover, often only one component of the response function is directly calculated [11,12], while the other component is obtained with the Kramers-Kronig relations, which may lead to increasing inaccuracies.

For practical reasons, simplified approaches such as the Drude [16] or the Drude-Lorentz (DL) description are often used. The DL model provides a comprehensive framework

for modeling the optical response of various materials as it incorporates interband transitions. It has been widely used [17–21], is flexible, and can be easily implemented for different materials. Most importantly, its fast predictions allow for quick analysis of experiments. Recently, the DL model has been fitted to data for gold obtained by DFT calculations [14].

Here, we develop an extension of the DL model to study the temperature-dependent optical properties of highly excited gold for a broad range of probe frequencies. In contrast to Ref. [14], we start with a fit to the measured dielectric function at room temperature [22] and smoothly extend it to higher temperatures. To obtain the optical response at elevated temperatures, we apply temperature-dependent collision frequencies in the Drude part [23]; i.e., the intraband response is fully determined by the temperature-dependent occupation of the conduction band and the changing Drude damping. For the interband response, we introduce an additional temperature dependence of the Lorentz oscillators. In our approach, we connect the amplitudes of the Lorentz oscillators with the density of oscillating electrons at constant oscillator positions. The resonance energies are modified according to the shift of the chemical potential and the broadening of the Fermi edge at elevated temperatures. The remaining freedom for the Lorentz parameters can be fixed by comparison with DFT-based calculations and experiments. Finally, the damping of the Lorentz oscillators is described in the same way as the Drude damping, taking into account electron-phonon and electron-electron scattering. In this way, our model allows for a direct transfer of the parameters describing Lorentz oscillators at room temperature to a description applicable to gold with highly excited electrons.

Our results show strong changes in the intra- and interband contributions to the dielectric function. Moreover, our model reproduces features in the reflectivity of highly excited gold

*ndione@rptu.de

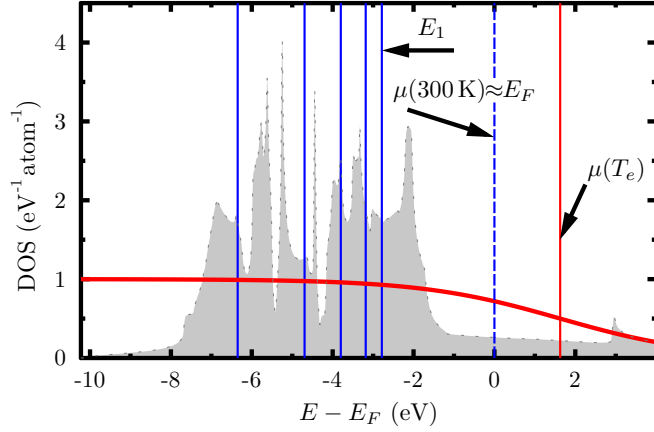


FIG. 1. Total density of states of gold. The Fermi energy E_F is plotted as a blue dashed line and sets the zero point of the energy scale. A Fermi distribution for $T_e = 2 \times 10^4$ K and the chemical potential at this temperature are plotted with red solid lines. The resonance energies E_j (Lorentz oscillators) considered in this work are highlighted with blue solid lines.

that have been found with extensive DFT-based calculations [24]. Applying our methods to thin gold films, we find a strong nonlinear dependence of the optical properties on the electron temperature. These changes are more pronounced at photon energies below the interband threshold and, particularly, for p -polarized light, making such a setup ideal for probing.

II. THEORETICAL FRAMEWORK

We consider the excitation of matter by a short pulse of infrared or optical light. For noble metals like gold, such excitations involve only the two upper electron bands, i.e., the $5d$ valence and the $6sp$ conduction electrons. In general, both types of electrons contribute to the optical properties, but the low-frequency behavior is dominated by the $6sp$ electrons [22]. The density of states (DOS) can be calculated by density functional theory. Figure 1 shows results for gold as obtained by the Elk code [25] as well as the occupation of these states for a finite temperature. By projection, the partial density of states for d and sp electrons can be obtained as well (see, e.g., Ref. [26]). This projection may introduce inaccuracies. We resolve these small numerical inconsistencies by normalizing each partial DOS to yield one conduction electron and ten d -band electrons at room temperature, respectively.

The model we present here focuses on timescales when the electron distribution is relaxed and can be described with a temperature. This assumption is often satisfied for excitations with sufficiently high energy, where the kinetic stage establishing a Fermi distribution lasts only a few femtoseconds [27,28]. Here, the sp and d electrons are assumed to share the same temperature T_e and chemical potential μ ; i.e., we have

$$f(E, T_e, \mu) = \frac{1}{\exp[(E - \mu)/k_B T_e] + 1} \quad (1)$$

over both bands. Note that this assumption may not hold on timescales when a common electron temperature has been reached but the band occupation has not fully equilibrated [10,29]. The equilibration of the band occupation is, however,

much faster than the electron-phonon relaxation; thus there is an extended stage with a joint Fermi distribution (1) over both bands where most of the absorbed laser energy is contained in the electronic system. This stage with electron-phonon nonequilibrium is the main focus of interest for our current investigation.

The complex-valued dielectric function is a central and intrinsic quantity to describe how the material responds to an external electromagnetic field, such as a laser pulse. From this quantity, material properties such as reflection, conductivity, or absorption can be calculated directly [30]. The dielectric function is determined by the electron states specific to the material, i.e., the band structure. For metals like gold with a d -band character, the total dielectric function is a combination of intra- and interband contributions: $\epsilon_{\text{tot}} = \epsilon_{\text{intra}} + \epsilon_{\text{inter}}$. While the intraband response is dominated by the sp electrons, the interband response depends on the occupation within the d band.

A. Intraband response

In the optical limit with negligible momentum transfer from the photons, the intraband response for the electrons can be modeled with the Drude theory [16]

$$\epsilon_{\text{intra}}(\omega, T_i, T_e) = \epsilon_{\infty} - \frac{\omega_p^2(T_e)}{\omega^2 + i\omega\nu(T_i, T_e)}, \quad (2)$$

where ω is the frequency probed, ω_p denotes the plasma frequency, and ν is the collision or damping frequency, which depends on both the phonon and electron temperatures T_i and T_e , respectively. The background dielectric constant ϵ_{∞} differs from unity in noble metals and is $\epsilon_{\infty} = 3.104$ for gold [20].

The plasma frequency sets the frequency of collective electron excitations and is defined by the density of sp electrons via $\omega_p^2(T_e) = e^2 n_{sp}(T_e)/\epsilon_0 m_{sp}^*$ with e being the electron charge, ϵ_0 the vacuum permittivity, and m_{sp}^* the effective mass of the conduction electrons. For the latter, the free-electron mass is a good approximation in gold [22]. In our case, the plasma frequency becomes temperature-dependent as thermal excitations increase the sp density,

$$n_{sp}(T_e) = \int dE f(E, T_e, \mu) D_{sp}(E), \quad (3)$$

where $D_{sp}(E)$ is the partial DOS of the $6sp$ band.

The Drude damping in Eq. (2) is a key parameter when modeling the optical and transport properties of highly excited metals [23,24,26]. Its main contributions in gold are electron-phonon and electron-electron scattering rates. Thus, we have $\nu_{\text{tot}} = \nu_{ei}(T_i) + \nu_{ee}(T_e)$. At room temperature, it is dominated by the scattering of the sp electrons with the lattice phonons, as Pauli blocking prohibits scattering with d electrons. It is set in this work to match the experimental data of Johnson and Christy [22]. For a heated lattice, we assume ν_{ei} to increase linearly with T_i . For the description of ν_{ee} , we follow the model presented in Refs. [23,26] which takes into account the temperature dependence of the d -band hole and sp -band electron densities. At elevated T_e , the scattering of sp electrons by d electrons is the dominant damping mechanism and depends strongly on the number of conduction electrons [23], given by

TABLE I. Fit parameters of the Lorentz oscillators at room temperature. $\hbar\Gamma_{j,0}$, $\hbar\omega_{j,0}$, and $\hbar a_{j,0}$ are given in eV.

j	1	2	3	4	5
$\hbar a_{j,0}$	4.577	4.999	12.281	24.999	34.999
$\hbar\Gamma_{j,0}$	0.499	0.699	0.999	1.651	2.190
$\hbar\omega_{j,0}$	2.784	3.183	3.799	4.695	6.349

Eq. (3). Details for the description of the Drude damping are given in Ref. [26].

B. Interband response—room temperature

Photons with energies larger than the interband threshold can excite d -band electrons into the empty states of the conduction band. Strictly speaking, such interband processes should be treated using the matrix elements that describe the effect of light on the electrons as well as the density of states [31]. However, the Lorentz model provides a simplified way to describe the interband response and it has been applied frequently to materials at room temperature [17,20,32].

In the Lorentz model, valence electrons are assumed to be bound to the nucleus similarly to a spring. The model mimics the motion of electrons around their equilibrium positions with a damped harmonic oscillator driven by an electric field. These oscillators have specific resonance frequency, amplitude, and damping. The inclusion of damping in the Lorentz model implies that the electrons change their state, e.g., via collisions. The damping broadens the absorption line to a finite width [31], which also avoids singularities at the resonance frequency. Most materials have multiple characteristic resonances and the total response is a sum over all transitions possible in the optical medium. In the framework of this approach, the interband response can be written as [20]

$$\varepsilon_{\text{inter}}(\omega) = \sum_j \frac{a_{j,0}}{\omega_{j,0}^2 - \omega^2 - i\omega\Gamma_{j,0}}, \quad (4)$$

where $a_{j,0}$, $\omega_{j,0}$, and $\Gamma_{j,0}$ are the amplitude, the resonance frequency, and the damping of the Lorentz oscillators, respectively. Here, we choose to apply five Lorentz oscillators. This number is phenomenological and may be optimized to the energy spectrum of interest. An important property of the Lorentz dielectric function is the fact that it fulfills the Kramers-Kronig relations as long as the values of $\Gamma_{j,0}$ are positive [19,33].

For gold at room temperature, we obtain the Lorentz parameters $a_{j,0}$ and $\Gamma_{j,0}$ through a fit to experimental data [22]. The resulting parameters are summarized in Table I. The five resonance frequencies used here were taken from Ref. [20]. Figure 1 shows the position of the resonance energies $E_j = -\hbar\omega_{j,0}$ (blue vertical lines) in relation to the density of states. Here, and for the values given in Table I, we choose the Fermi energy E_F to be the zero point of our energy scale.

C. Interband response—excited matter

The application of the DL model to excited matter is not straightforward. As for the intraband response, we have to

account for modifications due to electron and phonon temperatures [34]. In particular, new transitions become possible as an increasing number of free states are created below the Fermi energy when the temperature rises. We propose here to keep the form of the interband response described by Eq. (4), but introduce temperature-dependent Lorentz parameters. Recently this approach has been applied to electron-phonon nonequilibrium by fitting the Lorentz model to results obtained by DFT at distinct elevated electron temperatures [14]. Our approach aims to introduce a temperature dependence to the strength and damping of the Lorentz oscillators in a smooth way by taking into account the changing occupation numbers in the two optically active bands. The oscillator positions will be kept constant with respect to the density of states. In this way, we provide an easy-to-use description that is smoothly connected to the values at room temperature and might also be applied in nonequilibrium.

We start by considering the amplitudes of the Lorentz oscillators a_j . This parameter can be connected to the number of oscillating d -band electrons [35]. Thus, we scale a_j with the electron occupation at the oscillator position in the d band normalized to the value at 300 K,

$$a_j(T_e) = a_{j,0} \frac{n_d^{E_j}(T_e)}{n_d^{E_j}(300 \text{ K})}. \quad (5)$$

Here, $n_d^{E_j}(T_e)$ is the density of electrons in the d band within an energy interval $[E_j - \Delta, E_j + \Delta]$ that contains the energy E_j of the oscillator j ,

$$n_d^{E_j}(T_e) = \int_{E_j - \Delta}^{E_j + \Delta} dE f(E, T_e, \mu) D_d(E), \quad (6)$$

where D_d is the partial DOS of the d band. Δ represents a small energy interval. Thus, we can apply the mean value theorem for integrals to Eq. (6) and obtain that the amplitude is proportional to the distribution function at the oscillator position E_j ,

$$a_j(T_e) = a_{j,0} \frac{f(E_j, T_e)}{f(E_j, 300 \text{ K})}. \quad (7)$$

Next, we focus on the temperature dependence of the resonance frequencies. When the electron temperature rises, holes are created in the d band below E_F as more and more d -band electrons are thermally excited into the conduction band, which becomes increasingly populated. Moreover, the chemical potential μ also shifts at elevated temperatures, which reflects the conservation of the total number of particles. The details of the shift depend on the shape of the DOS around E_F . In the case of gold, the DOS exhibits high d -band peaks below E_F whereas considerably fewer states exist above the Fermi energy (see Fig. 1). Thus, the chemical potential for gold rises with increasing electron temperature [24]. An example for the chemical potential at $T_e = 2 \times 10^4$ K and the corresponding Fermi distribution is plotted in Fig. 1 (red lines).

This shift of the chemical potential renders interband transitions more difficult as the d electrons need to overcome a broader energy gap. However, the broadening of the Fermi edge facilitates the transitions from d into sp states below the chemical potential as not all of these are fully occupied

any more; i.e., we see a softening of the Pauli blocking with rising electron temperature. To account for both effects, the resonance frequencies are modified according to

$$\hbar\omega_j(T_e) = \hbar\omega_{j,0} + \Delta\chi(T_e), \quad (8)$$

where $\Delta\chi(T_e) = \chi(T_e) - \chi(300 \text{ K})$ is the temperature-dependent shift from the fixed basis points of the Lorentz oscillators to the lowest available state for the conduction band. The function χ is set to be

$$\chi(T_e) = \mu(T_e) - ck_B T_e. \quad (9)$$

The first term accounts for the temperature dependence of the chemical potential and the second term for the temperature broadening of the Fermi edge. The constant c sets the strength of the second effect. It can be fixed by comparison to experimental data or first-principles simulations.

Finally, the damping parameters are considered. We describe their temperature dependence similarly to the Drude damping, i.e., including electron-phonon and electron-electron scatterings,

$$\Gamma_j(T_i, T_e) = \Gamma_{ei}^j(T_i) + \Gamma_{ee}(T_e). \quad (10)$$

At room temperature, the electron-phonon damping Γ_{ei}^j dominates, and their value is identical to $\Gamma_{j,0}$ presented in Table I. For elevated temperatures, one can assume a linear increase with the lattice temperature. However, we consider cases where the probe time is fast and the lattice remains cold; i.e., the damping due to scattering with phonons remains unchanged here. In contrast, the damping due to electron-electron scattering Γ_{ee} is strongly varying with electron temperature via changes in the occupation of the d and sp bands. Here, we propose to use the same form as for the intraband part, since the damping of the interband transitions relies on the same scattering process [23,26].

To summarize our model, we propose a description of the dielectric function employing the Drude-Lorentz form with temperature-dependent oscillator frequencies, amplitudes, and damping terms, thus describing intraband and interband contributions. For the Drude part, that is, for the intraband contributions, this extension to high temperatures has been shown to work well and to agree with experimental data [10,23,26]. The Lorentz part, describing transitions between bands, will be discussed against DFT-based data in the following section. Despite its simplicity, the model is able to reproduce many features of the optical properties of excited gold with very low computational effort.

III. RESULTS AND DISCUSSION

We present the results of our analysis of the dielectric function and derive the optical properties of gold for cases with hot electrons and cold phonons. We also compare our results with calculations based on DFT and use this comparison to fix the free parameter in the DL model. Applying our methods to thin films reveals more detailed insights into the optical properties and points toward potential applications in various fields.

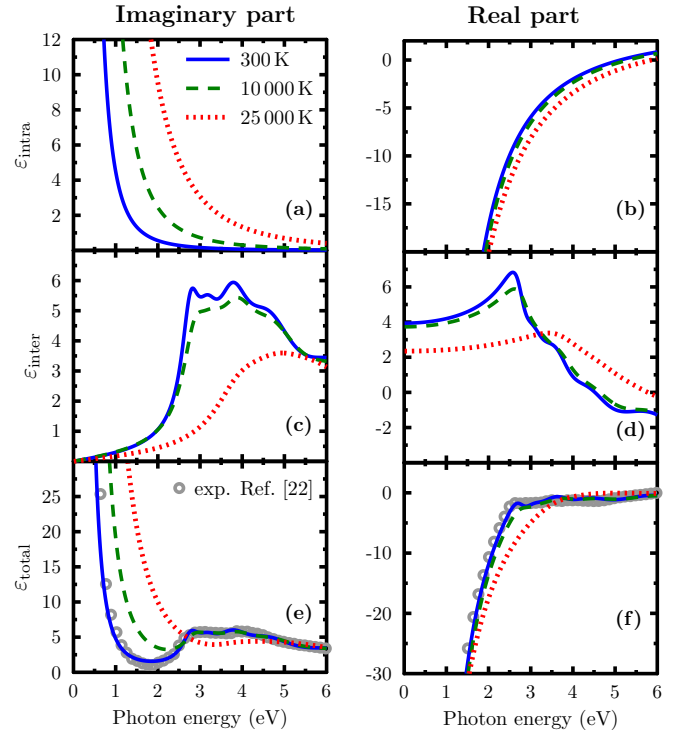


FIG. 2. Broadband dielectric function of gold for three electron temperatures. Imaginary part (left panels) and real part (right panels). Panels (a) and (b) show intraband (Drude) response, (c) and (d) interband (Lorentz) part, and (e) and (f) the total response. The experimental data at room temperature are taken from Ref. [22].

A. Temperature-dependent dielectric function

We examine the dielectric function of gold across a broad spectral range to cover absorption of and probing by photons of different energy. Figure 2 shows the dielectric function in dependence on the photon energy for various electron temperatures while keeping the phonons at 300 K. The individual intra- and interband contributions are shown in Figs. 2(a) to 2(d). The intraband part is calculated with Eq. (2) and the interband response is determined by Eq. (4). The total dielectric function, i.e., the sum of both contributions, is shown in Figs. 2(e) and 2(f).

At room temperature and photon energies in the infrared regime, the imaginary part of the dielectric function is dominated by intraband contributions, i.e., the Drude response of free carriers as interband transitions are very unlikely; compare Figs. 2(a) and 2(c). However, this is not true for the real part that has positive and non-negligible interband contributions at low photon energy, as depicted in Fig. 2(d) and in qualitative agreement with the findings of Ref. [36]. That is, the Drude model may not be sufficient to describe the real part of the dielectric function of gold even for the small photon energies.

With the onset of interband transitions, i.e., for photon energies around 1.9 eV, the imaginary part of the interband (Lorentz) response increases significantly as shown in Fig. 2(c). The real part, plotted in Fig. 2(d), shows a maximum at a photon energy equal to the first resonance energy $\hbar\omega_{1,0}$, before decreasing at higher photon energies. In

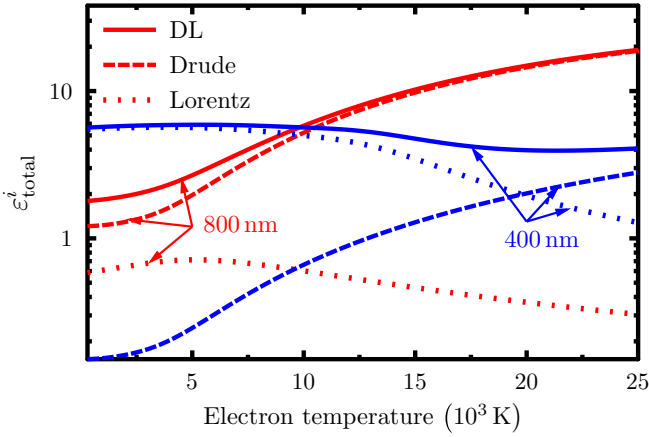


FIG. 3. Imaginary part of the dielectric function of Au in dependence on the electron temperature at laser wavelengths of 800 nm (red) and 400 nm (blue). Intraband parts (dashed lines), interband contributions (dots), and total (solid lines). Note the logarithmic scale on the vertical axis.

contrast, the imaginary part of the intraband (Drude) contribution decreases monotonically, while its real part increases; see Figs. 2(a) and 2(b).

The total dielectric response function, Figs. 2(e) and 2(f), shows a Drude-like behavior for energies below the onset of interband transitions and is relatively flat above ~ 3 eV. We take the experimental data of Ref. [22] (gray circles) as a reference at 300 K and match these data reasonably well with the fit parameters in Table I.

At elevated electron temperatures, we observe a strong enhancement of interband contributions in the imaginary part over the entire spectrum, plotted in Fig. 2(a) for 10 000 K and 25 000 K. We attribute this enhancement to a strong rise of both the Drude damping and the plasma frequency [26]. In contrast, the temperature effects on the real part of the Drude response are small.

The interband (Lorentz) response also varies with the electron temperatures. It is calculated using Eqs. (4)–(10) and by setting $c = 1/2$ in Eq. (9), we include the temperature broadening of the Fermi edge in the sp band. The imaginary part becomes smaller for increasing electron temperatures, as can be seen in Fig. 2(c). This behavior is expected: With rising T_e the chemical potential shifts to higher energies, increasing the resonance frequencies and thus decreasing the probability of transitions. The real part of the interband response decreases at low energies as well. Moreover, the main resonance peak shifts to higher energies [see Fig. 2(d)]. Due to the softer decrease of the distribution function at the chemical potential, the transition peaks are more and more washed out at elevated T_e , leading to smoother interband curves, where the changes in the individual contributions are stronger at photon energies below the interband transition threshold. Figures 2(e) and 2(f) show that the total dielectric function is considerably modified at these smaller photon energies, whereas it changes just slightly above the threshold. Such behavior is in qualitative agreement with previous observations for copper obtained by the Kubo-Greenwood formalism [12].

Figure 3 shows the important imaginary part of the dielectric function in dependence on the electron temperature T_e for two fixed laser wavelengths: 800 nm (1.55 eV) and 400 nm (3.1 eV). At room temperature, the Drude part dominates the total dielectric function $\epsilon''_{\text{total}}$ for the long wavelength, i.e., low photon energy, while the Lorentz contribution is very small but finite. Driven by the Drude contribution, $\epsilon''_{\text{total}}$ increases nonlinearly for increasing electron temperatures. The behavior for the short wavelength of 400 nm is quite different. For low electron temperatures, the Lorentz part dominates, and the value of $\epsilon''_{\text{total}}$ is relatively constant, before it starts a minor decline toward a minimum around 20 000 K, where the Drude and Lorentz curves intersect. Above this temperature, $\epsilon''_{\text{total}}$ increases again, which is not very visible due to the logarithmic scale of Fig. 3. This rise is attributed to a strong enhancement of the Drude part.

To understand this behavior, it is essential to assess individual contributions. According to Eq. (2), $\epsilon''_{\text{intra}}$ is proportional to ν and ω_p^2 . Thus, its trend is fully defined by changes in the collision frequency ν and the plasma frequency ω_p . At sufficiently high T_e , a significant number of d electrons are thermally excited into free states of the sp band and create holes below E_F . These holes allow for efficient electron-electron scattering and, thus, considerably increase the Drude damping ν [23,26]. Combined with an increase in the plasma frequency, the intraband response rises. The interband response, on the other hand, shows an overall decrease with increasing temperature. This results from a lower probability of electron transitions as the chemical potential and, thus, the interband excitation threshold rises with temperature. Here, we note that the resonance frequencies are the most critical parameters in the Lorentz approach.

Figure 4 shows the imaginary part of the dielectric function in gold calculated with our DL model as well as results from two different DFT approaches [14,24]. At room temperature, the results of the DL model are fitted to experimental data [22], obtaining the parameters in Table I. Both DFT results predict a similar trend to the experimental data, but show significant quantitative deviations, especially for photon energies between 2 and 4 eV. The results of Silaeva *et al.* [14] also exhibit a shift toward lower energies. Such a shift was previously also reported for the real part of the AC conductivity [11] and explicitly attributed to the approximation level used for the exchange-correlation part of the energy functional. The results of Blumenstein *et al.* [24] show a better match to the experimental data in the infrared region since they use the Drude damping as an adjustable parameter.

Figures 4(b) and 4(c) compare our DL model with the results of the quantum simulations [14,24] for elevated electron temperatures. Setting $c = 1/2$ in Eq. (9), the DL model compares reasonably well with the DFT-based results. All results maintain similar shapes over a wide range of temperatures and the main features remain consistent. However, the quantitative deviations seen at room temperature persist as well, especially between 2 and 4 eV. The discrepancies at elevated temperatures are thus inherited from the deviations at 300 K.

If we neglect the thermal broadening, i.e., using $c = 0$ (dotted curves in Fig. 4), the deviations between the DL model and the DFT results are more pronounced. In this case, the dip of the dielectric function above 2 eV is stronger, since the

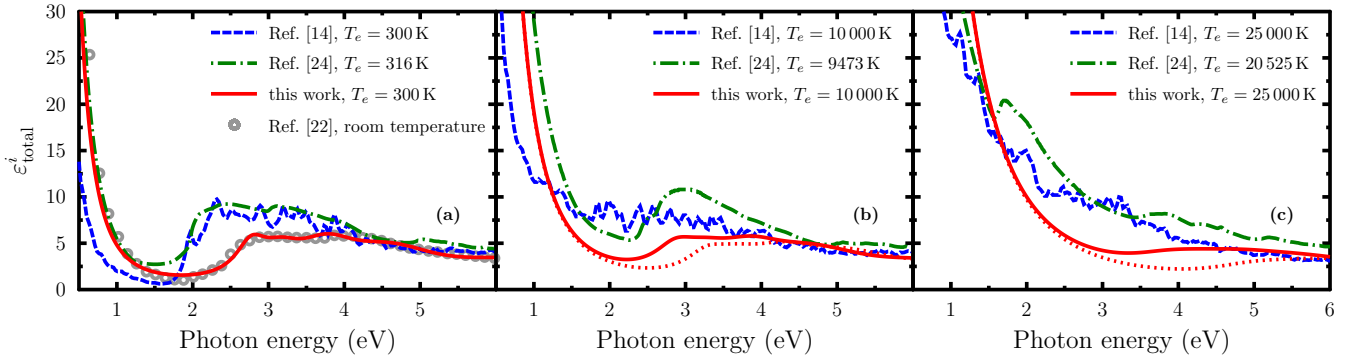


FIG. 4. Imaginary part of the dielectric function of gold as a function of photon energy. The results obtained with the Drude-Lorentz model (red curves) are compared with the DFT-based calculations of Ref. [24] (green dashed-dotted curves) and the *ab initio* calculations of Ref. [14] (blue dashed lines). Panel (a) shows the room temperature case, including experimental data from Ref. [22] (gray circles). Panels (b) and (c) are for elevated electron temperatures, where the solid red line and red dots apply $c = 1/2$ and $c = 0$ in Eq. (9), respectively.

full gap is taken into account; i.e., interband transitions are more difficult. The comparison emphasizes the importance of refining theoretical models and calls for dedicated high-temperature experiments or improved *ab initio* simulations.

B. Broadband reflectivity of bulk gold

The reflectivity of materials is a measurable quantity and can serve as a benchmark for models. It can be directly calculated from the dielectric function discussed above. Under normal incidence, the surface reflectivity is determined as

$$R(\omega, T_i, T_e) = \left| \frac{\tilde{n}(\omega, T_i, T_e) - 1}{\tilde{n}(\omega, T_i, T_e) + 1} \right|^2, \quad (11)$$

where \tilde{n} is the complex refractive index and is related to the dielectric function via $\tilde{n} = \sqrt{\epsilon}$.

For the following results, we use the Drude-Lorentz form of the dielectric function developed in Sec. II and, as before, keep the phonons at room temperature. Figure 5 displays the reflectivity of bulk gold as a function of electron temperature and photon energy. For Fig. 5(a), we set $c = 1/2$ in Eq. (9), whereas for the results in Fig. 5(b) the value $c = 0$ is used.

This means that the temperature broadening of the Fermi edge is applied in the left panel, whereas it is neglected in the middle panel, where only the shift of the chemical potential is applied. Accordingly, transitions of *d* electrons are easier in the former case as additional free states are available around the Fermi edge. We compare both results with data from DFT-based calculations [24] plotted in Fig. 5(c).

At room temperature, bulk gold is highly reflective below the onset of interband transition energy of ~ 1.9 eV. Above this energy, absorption of photons by *d* electrons starts to increase strongly, and this effect decreases the reflectivity. With increasing electron temperature, the reflectivity decreases in the infrared regime. Our results depicted in Fig. 5(a) show a redshift of the reflectivity edge for increasing temperatures up to ~ 5000 K. This results from the term $\Delta\chi$ in Eq. (8) being negative for $c = 1/2$ at these low temperatures; i.e., the softening of the Fermi edge dominates the increase of the chemical potential. The results in Fig. 5(b) follow by disregarding the softening of the Fermi edge ($c = 0$) and do not show a redshift of the reflectivity edge. There is, however, experimental evidence for such a redshift in gold, where the onset of interband transitions decreases when the temperature

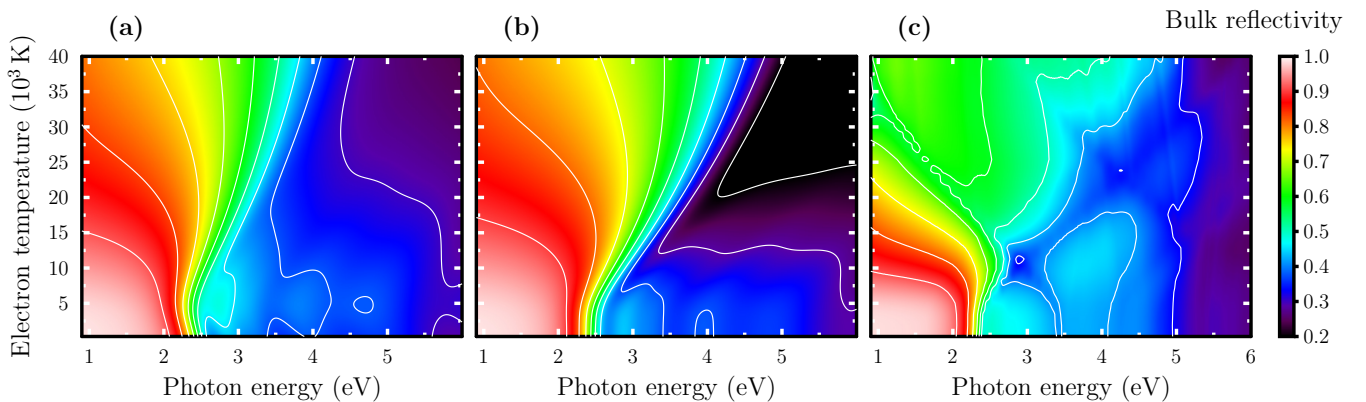


FIG. 5. Surface reflectivity of bulk gold versus electron temperature and photon energy. Panel (a) uses $c = 1/2$ in Eq. (9), i.e., including a temperature broadening of the Fermi edge for the lowest available state. In panel (b) we consider $c = 0$; i.e., the lowest available state in the *sp* band is determined only by $\mu(T_e)$. The right panel (c) shows results of DFT-based calculations from Ref. [24].

is raised from 90 K to 725 K [37]. Similar results have been found for silver [38]. These results show the importance of the broadening of the Fermi edge in the model.

For higher electron temperatures, the chemical potential increases significantly and shifts the lowest available sp state toward higher energies. Thus, the reflectivity edge experiences a blueshift. This can be observed in all three panels of Fig. 5, and is most pronounced in Fig. 5(b), where no broadening of the Fermi edge is considered and, thus, the full energy gap is accounted for. Furthermore, Fig. 5(b) shows a strong decrease of reflectivity for high photon energies and increasing temperatures, which is, however, absent in the DFT-based results plotted in Fig. 5(c). Moreover, we see that the edge in the reflectivity is smeared out at elevated T_e , which is also visible in the DFT-based results of Fig. 5(c). Once again, this effect is mainly attributed to the softening of the distribution function. For photons in the infrared regime and at very high temperatures, our calculations differ from the results of Ref. [24] depicted in Fig. 5(c). While the damping of the intraband contribution included in Ref. [24] has been adapted by comparison with a measured integrated self-reflectivity, our approach has led to a good agreement with THz measurements at high temperatures [9,26].

Overall, the inclusion of the softening of the Fermi edge by the choice of $c = 1/2$ in Eq. (9) leads to a reasonable agreement of our calculations with experimental insights in the low-temperature regime as well as with DFT-based data for elevated temperatures; compare Figs. 4 and 5. We therefore take $c = 1/2$ in Eq. (9) as the best option for future calculations. Our approach requires significantly less computational effort than DFT-based calculations and its Drude part has been validated by THz data for high temperatures. Therefore, we conclude that our model provides a reasonably accurate, efficient, and easily applicable approximation for the behavior of the optical response in highly excited gold including intra- and interband transitions.

C. Application to thin films

Many experiments applying laser excitation have been performed on thin films. This approach avoids temperature gradients as the foil can be homogeneously heated by ballistic electrons [8,39–41]. To calculate the reflectivity, transmissivity, and absorption of a freestanding thin gold film, we apply multiple-reflection theory [30]. We assume a single gold layer with two parallel surfaces and vacuum at both interfaces of the thin film, like, e.g., used in Refs. [8,39,42]. We label the vacuum parts with indices 1 and 3, respectively, and the gold film is indexed with 2 leading to [30]

$$R(\omega, T_i, T_e) = \left| \frac{r_{12} + r_{23}e^{i2\beta}}{1 + r_{12}r_{23}e^{i2\beta}} \right|^2, \quad (12a)$$

$$T(\omega, T_i, T_e) = \left| \frac{t_{12}t_{23}e^{i\beta}}{1 + r_{12}r_{23}e^{i2\beta}} \right|^2 \frac{n_3 \cos(\theta_3)}{n_1 \cos(\theta_1)}, \quad (12b)$$

where r_{km} and t_{km} are the reflection and transmission coefficients of light propagating from medium k to medium m . These coefficients are determined by the Fresnel equations [30]. In our case, n_1 and n_3 are the refractive indices of the vacuum and are thus equal. θ_1 is the angle of

incidence, and θ_3 is the angle between the transmitted light and the surface normal ($\theta_1 = \theta_3$ because media 1 and 3 are both vacua). The quantity $\beta = 2\pi h \cos(\theta_2)n_2/\lambda$ denotes the phase change of light resulting from multiple internal reflections. Here, λ is the wavelength of the probe pulse, h is the film thickness, and θ_2 is the refracted angle of light within the gold film (medium 2) after entering from vacuum (medium 1). n_2 is the complex refractive index of gold calculated with the temperature-dependent dielectric function described above.

Figure 6 shows the reflectivity R (top row), transmissivity T (middle row), and absorption $A = 1 - R - T$ (bottom row) of a freestanding gold film with 25 nm thickness as a function of the probed photon energy and the electron temperature. We present the results for normal incidence in the left columns. For the results shown in the central and right columns, we consider an angle of incidence of $\theta_1 = 45^\circ$, where panels (b), (e), and (h) of Fig. 6 are for s -polarized light and panels (c), (f), and (i) assume p -polarized light.

At 300 K, the thin film reflects less light than the bulk material for all considered cases. Moreover, the reflectivity edge is lower and less pronounced for the thin film, especially for the p -polarized light. As T_e increases, the reflectivity decreases in the infrared regime. The s -polarized light is more reflective over the whole spectrum compared to the p -polarized light, whose reflectivity shows enhanced features. Similar to bulk, we also observe a blueshift of the reflectivity edge and its broadening at elevated electron temperatures.

The effect of elevated electron temperature on the transmissivity is relatively low, except for photon energies between ~ 1 and ~ 3 eV. The transmissivity maps all show a peak around ~ 2.4 eV, which decreases and shifts toward higher energies with increasing T_e . These features appear at normal incidence and for both polarizations considered, but are more pronounced for the p -polarized light.

Since the transmissivity is low, the absorption is more or less the inversion of the reflectivity. For small photon energies below the absorption edge, the absorption at room temperature is very low (less than 6%), but increases significantly with increasing temperature. In contrast, the absorption is large for higher photon energies, due to the possibility of transferring d electrons into free states of the sp band, and appears to be nearly independent of temperature. Similar to the reflectivity, we also observe a shift of the absorption edge and its broadening.

Our results for thin films show a similar qualitative behavior of the optical parameters for normal and for oblique incidence, but with large differences in magnitude. Moreover, some of the features observed for R , T , and A are much more pronounced for p -polarized light than for s -polarized light. The latter is thus more sensitive and seems to be ideal for probing changes in the optical properties. Figure 6 also reveals that photon energies below the interband threshold are better suited to detect changes in material properties than higher photon energies.

The dependence of the optical properties on electron temperature is difficult to assess quantitatively in Fig. 6. We thus highlight it for two fixed probe wavelengths, one below and one above the interband threshold. Figure 7 shows the reflectivity and absorption for p -polarized light as a function of the electron temperature for a gold film of 25 nm thickness.

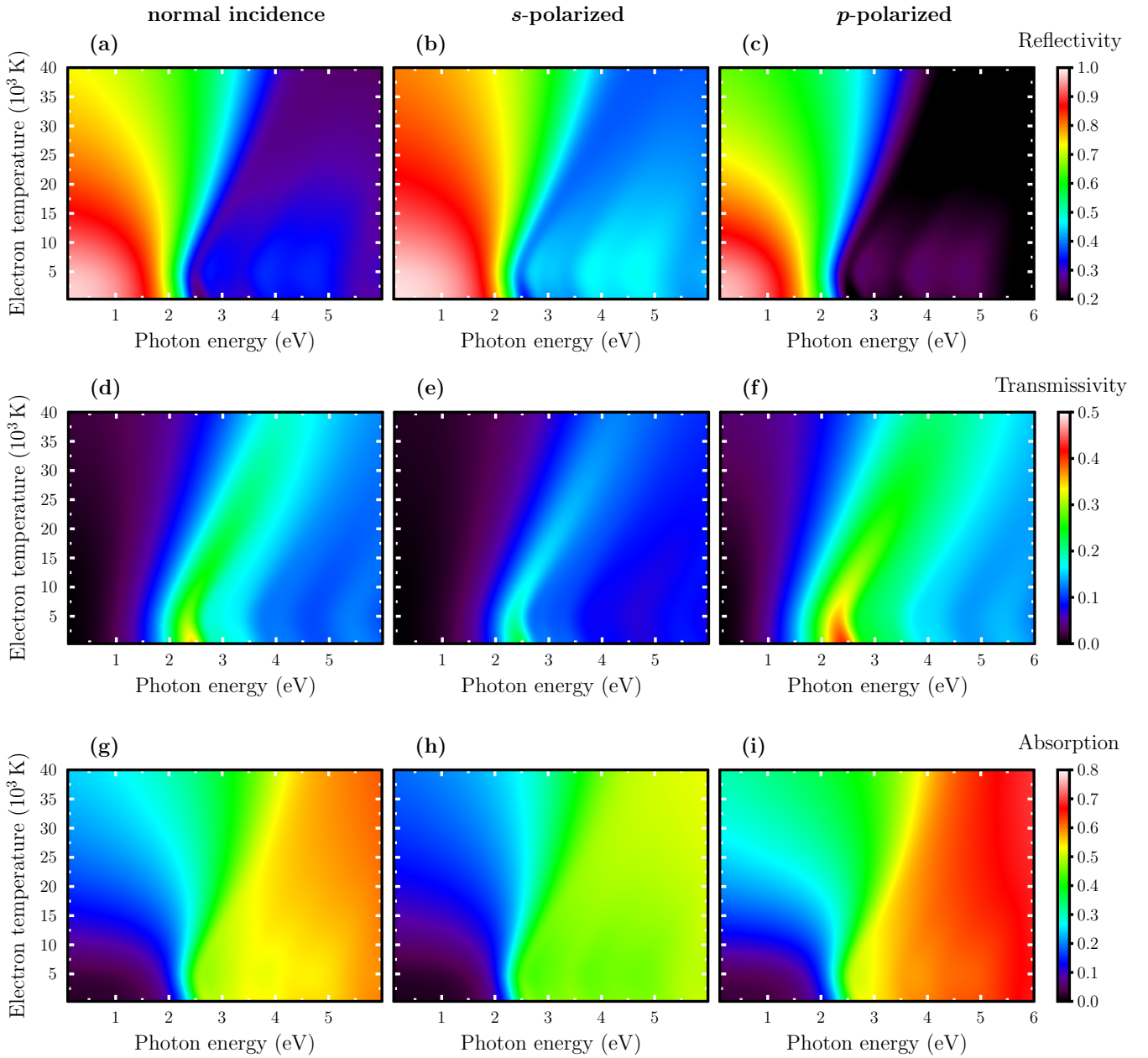


FIG. 6. Reflectivity (top row), transmissivity (middle row), and absorption (bottom row) of a 25 nm thin freestanding gold film as a function of electron temperature and photon energy. The results shown in the left vertical column are calculated for light at normal incidence. The panels in the central and right vertical columns are calculated for s - and p -polarized light, respectively, with an angle of incidence of $\theta_1 = 45^\circ$.

We consider probe wavelengths of 800 nm (1.55 eV) and 400 nm (3.1 eV). Depending on wavelength, we observe a different qualitative behavior of reflectivity and absorption. For 800 nm, the reflectivity decreases with increasing T_e . This is due to an increase in the number of free states below E_F . In contrast, for 400 nm, Fig. 7(b) shows a small increase in R when gold is heated. This is followed by a small decrease reaching a minimum at about $\sim 15\,000$ K before R experiences a larger increase. The increase in reflection is due to a decrease in the number of free states above the Fermi level with increasing T_e .

Equally interesting is the absorption shown in Fig. 7. For the 800 nm laser, the absorption increases nonlinearly with the electron temperature. At the highest temperature shown,

the absorption is more than five times larger than its initial value. That is, the absorption follows a trend similar to that of $\varepsilon_{\text{total}}^i$ shown in Fig. 3. At sufficiently high T_e , more d electrons, which serve as a reservoir, are excited above E_F and are responsible for the observed nonlinearity. For 400 nm, the absorption is nearly constant. The absorption only reduces slightly at very high T_e when many d electrons are thermally excited.

Overall, our calculations show the importance of considering temperature-dependent optical properties when modeling the optical response of thin films after ultrafast excitation. This behavior is particularly important when estimating the time-dependent absorption during transient energy deposition, especially for thin films. Probing with different polarizations

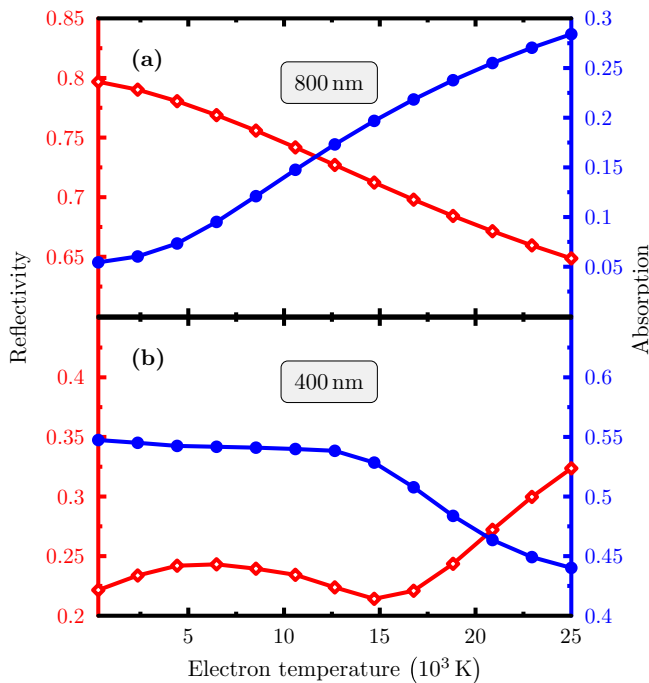


FIG. 7. Reflectivity and absorption of a 25 nm thin freestanding gold film for p -polarized light as a function of the electron temperature. (a) For a wavelength of 800 nm and (b) for 400 nm.

can also help to highlight features arising in heated matter and, thus, can be used for probing the states created.

IV. CONCLUSION

In summary, we have studied the optical properties of excited gold for a broad spectrum of probe frequencies and a large range of temperatures. We have developed our approach starting from the well-known Drude-Lorentz model fitted to experimental data for room temperature. For excited gold, we have generalized the description by introducing a temperature dependence into the resonance frequencies, amplitudes,

and damping. These parameters may depend on the electron temperature directly or via the occupation of electron states around the Fermi edge. The temperature dependence of the intraband response, i.e., the Drude part, has been applied as suggested in previous studies [23,26].

Our model shows a good qualitative agreement with data for excited gold obtained by DFT-based calculations [14,24]. In particular, it reproduces key features of the reflectivity well. Deviations in the energy range of 2–4 eV are due to the inability of the DFT approaches to match the experimental data at 300 K and relayed for higher electron temperatures. Compared to DFT simulations, a major advantage of our DL model is the strongly reduced computational effort, making it attractive for the analysis of experimental data and parameter scans.

When applied to thin gold films, our method reveals a high sensitivity of the reflectivity and absorption on the electron temperature. For both quantities, we observe a qualitatively different behavior for photon energies below and above the threshold for interband transitions with a larger sensitivity to electron temperature for low photon energies. Moreover, we find more pronounced features for p -polarized light which, thus, can be considered an ideal probe for investigating temperature effects.

The approach presented can easily be implemented in more complex numerical simulations that model the ultrafast processes during and shortly after the energy deposition with short laser pulse and, thus, offers valuable insights into these relaxation processes. It can be applied to materials with Fermi-distributed electrons as well as nonequilibrium situations. Although only results for a cold lattice are shown here, the effect of an excited phonon system can easily be included by incorporating damping due to electron-phonon scattering. Extensions of the present work toward materials with a similar band structure, such as copper and silver, are straightforward and require only the adjustment of a few parameters. While our current calculations use the ground state DOS, future investigations employing advanced simulation methods [43–45] could provide valuable insights and extend the applicability of our model for high electron temperatures.

-
- [1] M. Hartelt, P. N. Terekhin, T. Eul, A.-K. Mahro, B. Frisch, E. Prinz, B. Rethfeld, B. Stadtmüller, and M. Aeschlimann, Energy and momentum distribution of surface plasmon-induced hot carriers isolated *via* spatiotemporal separation, *ACS Nano* **15**, 19559 (2021).
- [2] P. N. Terekhin, J. Oltmanns, A. Blumenstein, D. S. Ivanov, F. Kleinwort, M. E. Garcia, B. Rethfeld, J. Ihlemann, and P. Simon, Key role of surface plasmon polaritons in generation of periodic surface structures following single-pulse laser irradiation of a gold step edge, *Nanophotonics* **11**, 359 (2022).
- [3] K. Sugioka and Y. Cheng, Ultrafast lasers—reliable tools for advanced materials processing, *Light: Sci. Appl.* **3**, e149 (2014).
- [4] R. K. Vinnakota and D. A. Genov, Terahertz optoelectronics with surface plasmon polariton diode, *Sci. Rep.* **4**, 4899 (2014).
- [5] T. Heilpern, M. Manjare, A. O. Govorov, G. P. Wiederrecht, S. K. Gray, and H. Harutyunyan, Determination of hot carrier energy distributions from inversion of ultrafast pump-probe reflectivity measurements, *Nat. Commun.* **9**, 1853 (2018).
- [6] C.-K. Sun, F. Vallée, L. H. Acioli, E. P. Ippen, and J. G. Fujimoto, Femtosecond-tunable measurement of electron thermalization in gold, *Phys. Rev. B* **50**, 15337 (1994).
- [7] M. Obergfell and J. Demsar, Tracking the time evolution of the electron distribution function in copper by femtosecond broadband optical spectroscopy, *Phys. Rev. Lett.* **124**, 037401 (2020).
- [8] Z. Chen, B. Holst, S. E. Kirkwood, V. Sametoglu, M. Reid, Y. Y. Tsui, V. Recoules, and A. Ng, Evolution of ac conductivity in nonequilibrium warm dense gold, *Phys. Rev. Lett.* **110**, 135001 (2013).
- [9] Z. Chen, C. B. Curry, R. Zhang, F. Treffert, N. Stojanovic, S. Toleikis, R. Pan, M. Gauthier, E. Zapolnova, L. E. Seipp,

- A. Weinmann, M. Z. Mo, J. B. Kim, B. B. L. Witte, S. Bajt, S. Usenko, R. Souffi, T. Pardini, S. Hau-Riege, C. Burcklen *et al.*, Ultrafast multi-cycle terahertz measurements of the electrical conductivity in strongly excited solids, *Nat. Commun.* **12**, 1638 (2021).
- [10] P. D. Ndione, S. T. Weber, D. O. Gericke, and B. Rethfeld, Nonequilibrium band occupation and optical response of gold after ultrafast XUV excitation, *Sci. Rep.* **12**, 4693 (2022).
- [11] B. Holst, V. Recoules, S. Mazevet, M. Torrent, A. Ng, Z. Chen, S. E. Kirkwood, V. Sametoglu, M. Reid, and Y. Y. Tsui, *Ab initio* model of optical properties of two-temperature warm dense matter, *Phys. Rev. B* **90**, 035121 (2014).
- [12] E. Bévilion, R. Stoian, and J. P. Colombier, Nonequilibrium optical properties of transition metals upon ultrafast electron heating, *J. Phys.: Condens. Matter* **30**, 385401 (2018).
- [13] N. Brouwer, V. Recoules, N. Holzwarth, and M. Torrent, Calculation of optical properties with spin-orbit coupling for warm dense matter, *Comput. Phys. Commun.* **266**, 108029 (2021).
- [14] E. Silaeva, L. Saddier, and J.-P. Colombier, Drude-Lorentz model for optical properties of photoexcited transition metals under electron-phonon nonequilibrium, *Appl. Sci.* **11**, 9902 (2021).
- [15] H. Zhang, S. Zhang, D. Kang, J. Dai, and M. Bonitz, Finite-temperature density-functional-theory investigation on the nonequilibrium transient warm-dense-matter state created by laser excitation, *Phys. Rev. E* **103**, 013210 (2021).
- [16] P. Drude, Zur Elektronentheorie der Metalle, *Ann. Phys. (Berlin, Ger.)* **306**, 566 (1900).
- [17] A. D. Rakić, A. B. Djurišić, J. M. Elazar, and M. L. Majewski, Optical properties of metallic films for vertical-cavity optoelectronic devices, *Appl. Opt.* **37**, 5271 (1998).
- [18] A. Vial, A.-S. Grimault, D. Macías, D. Barchiesi, and M. L. de la Chapelle, Improved analytical fit of gold dispersion: Application to the modeling of extinction spectra with a finite-difference time-domain method, *Phys. Rev. B* **71**, 085416 (2005).
- [19] M. Moskovits, I. Srnová-Šloufová, and B. Vlčková, Bimetallic Ag-Au nanoparticles: Extracting meaningful optical constants from the surface-plasmon extinction spectrum, *J. Chem. Phys.* **116**, 10435 (2002).
- [20] O. Peña-Rodríguez, Modelling the dielectric function of Au-Ag alloys, *J. Alloys Compd.* **694**, 857 (2017).
- [21] H. S. Sehmi, W. Langbein, and E. A. Muljarov, Optimizing the Drude-Lorentz model for material permittivity: Method, program, and examples for gold, silver, and copper, *Phys. Rev. B* **95**, 115444 (2017).
- [22] P. B. Johnson and R. W. Christy, Optical constants of the noble metals, *Phys. Rev. B* **6**, 4370 (1972).
- [23] C. Fourment, F. Deneuille, D. Descamps, F. Dorchies, S. Petit, O. Peyrusse, B. Holst, and V. Recoules, Experimental determination of temperature-dependent electron-electron collision frequency in isochorically heated warm dense gold, *Phys. Rev. B* **89**, 161110(R) (2014).
- [24] A. Blumenstein, E. S. Zijlstra, D. S. Ivanov, S. T. Weber, T. Zier, F. Kleinwort, B. Rethfeld, J. Ihlemann, P. Simon, and M. E. Garcia, Transient optics of gold during laser irradiation: From first principles to experiment, *Phys. Rev. B* **101**, 165140 (2020).
- [25] The Elk Code, <http://elk.sourceforge.net>.
- [26] P. D. Ndione, D. O. Gericke, and B. Rethfeld, Optical properties of gold after intense short-pulse excitations, *Front. Phys.* **10**, 856817 (2022).
- [27] B. Y. Mueller and B. Rethfeld, Relaxation dynamics in laser-excited metals under nonequilibrium conditions, *Phys. Rev. B* **87**, 035139 (2013).
- [28] E. P. Silaeva, E. Bevilion, R. Stoian, and J. P. Colombier, Ultrafast electron dynamics and orbital-dependent thermalization in photoexcited metals, *Phys. Rev. B* **98**, 094306 (2018).
- [29] P. D. Ndione, S. T. Weber, B. Rethfeld, and D. O. Gericke, Density response to short-pulse excitation in gold, *Contrib. Plasma Phys.* **59**, e201800186 (2019).
- [30] M. Born and E. Wolf, *Principles of Optics* (Pergamon Press, Oxford, 1980).
- [31] M. Fox, *Optical Properties of Solids*, 2nd ed. (Oxford University Press, New York, 2010).
- [32] J. Navarrete, C. Siefe, S. Alcantar, M. Belt, G. D. Stucky, and M. Moskovits, Merely measuring the UV-visible spectrum of gold nanoparticles can change their charge state, *Nano Lett.* **18**, 669 (2018).
- [33] M. Dressel and G. Grüner, *Electrodynamics of Solids: Optical Properties of Electrons in Matter* (Cambridge University Press, Cambridge, 2002).
- [34] Y. Ping, D. Hanson, I. Koslow, T. Ogitsu, D. Prendergast, E. Schwegler, G. Collins, and A. Ng, Broadband dielectric function of nonequilibrium warm dense gold, *Phys. Rev. Lett.* **96**, 255003 (2006).
- [35] E. J. Gamboa, L. B. Fletcher, H. J. Lee, U. Zastra, E. Galtier, M. J. MacDonald, M. Gauthier, J. Vorberger, D. O. Gericke, E. Granados, J. B. Hastings, and S. H. Glenzer, Single-shot measurements of plasmons in compressed diamond with an x-ray laser, *Phys. Plasmas* **22**, 056319 (2015).
- [36] A. Ng, P. Sterne, S. Hansen, V. Recoules, Z. Chen, Y. Y. Tsui, and B. Wilson, dc conductivity of two-temperature warm dense gold, *Phys. Rev. E* **94**, 033213 (2016).
- [37] P. Winsemius, M. Guerrisi, and R. Rosei, Splitting of the interband absorption edge in Au: Temperature dependence, *Phys. Rev. B* **12**, 4570 (1975).
- [38] S. T. Sundari, S. Chandra, and A. K. Tyagi, Temperature dependent optical properties of silver from spectroscopic ellipsometry and density functional theory calculations, *J. Appl. Phys.* **114**, 033515 (2013).
- [39] Z. Chen, Y. Y. Tsui, M. Z. Mo, R. Fedosejevs, T. Ozaki, V. Recoules, P. A. Sterne, and A. Ng, Electron kinetics induced by ultrafast photoexcitation of warm dense matter in a 30-nm-thick foil, *Phys. Rev. Lett.* **127**, 097403 (2021).
- [40] J. Hohlfeld, S.-S. Wellershoff, J. Güdde, U. Conrad, V. Jähnke, and E. Matthias, Electron and lattice dynamics following optical excitation of metals, *Chem. Phys.* **251**, 237 (2000).
- [41] Z. Chen, V. Sametoglu, Y. Y. Tsui, T. Ao, and A. Ng, Flux-limited nonequilibrium electron energy transport in warm dense gold, *Phys. Rev. Lett.* **108**, 165001 (2012).

- [42] T. Ao, Y. Ping, K. Widmann, D. F. Price, E. Lee, H. Tam, P. T. Springer, and A. Ng, Optical properties in nonequilibrium phase transitions, *Phys. Rev. Lett.* **96**, 055001 (2006).
- [43] E. Bévilion, J. P. Colombier, V. Recoules, and R. Stoian, Free-electron properties of metals under ultrafast laser-induced electron-phonon nonequilibrium: A first-principles study, *Phys. Rev. B* **89**, 115117 (2014).
- [44] Q. Zeng, B. Chen, X. Yu, S. Zhang, D. Kang, H. Wang, and J. Dai, Towards large-scale and spatiotemporally resolved diagnosis of electronic density of states by deep learning, *Phys. Rev. B* **105**, 174109 (2022).
- [45] P. Plettenberg, B. Bauerhenne, and M. E. Garcia, Neural network interatomic potential for laser-excited materials, *Commun. Mater.* **4**, 63 (2023).